Computational Materials Science 214 (2022) 111672

Contents lists available at ScienceDirect

Computational Materials Science

journal homepage: www.elsevier.com/locate/commatsci

Full Length Article

Hybrid exchange–correlation functionals for van der Waals $TiSe_2$ material: Parametrization versus a posteriori D3 dispersion corrections

Sergio Ricardo de Lazaro [a,*], Guilherme Bonifácio Rosa [a], Renan Augusto Pontes Ribeiro [b], Luis Henrique da Silveira Lacerda [c], Marisa Carvalho de Oliveira [d], Elson Longo [d]

[a] State University of Ponta Grossa (UEPG), Av. Gen. Carlos Cavalcanti, 4748, 84030-900 Ponta Grossa, Paraná, Brazil
[b] Minas Gerais State University (UEMG), Divinópolis, Minas Gerais, Brazil
[c] State University of Campinas (UNICAMP), Campinas, São Paulo, Brazil
[d] CDMF, Federal University of São Carlos (UFSCAR), São Carlos, São Paulo, Brazil

ARTICLE INFO

Keywords:
DFT
D3 Grimme
$TiSe_2$
Superconductor
Van der Waals
Hybrid

ABSTRACT

Superconductivity is one of the most interesting electrical phenomena found in Physical Science. The null electrical resistance provides a unique free displacement for the electrons into the material. $TiSe_2$ is a superconductor material below 4K, creating a charge density wave as electrical propagation. Gaussian basis sets or exchange–correlation functionals poorly described the high interaction distance as van der Waals force because of low exchange–correlation energy. One physical–mathematical tool to indicate long-range distance is the Grimme's or D3 dispersion. In this work, quantum simulations based on DFT using periodic models depicted in CRYSTAL17 code investigated the $TiSe_2$ material regarding PBE0, HSE06, and B3LYP functionals and Grimme's dispersion. In particular, the high covalent feature on the Ti–Se chemical bond is challenging for DFT functionals, while van der Waals interaction between lamellas is essential for crystalline structure. Then, relative errors quantified the functional descriptions to evaluate the influence of hybrid and parameterized hybrid functionals on this critical material's structural, electronic, and vibrational properties.

1. Introduction

Electrical transmission in populated areas is a complex process, such as power plants, power lines (transmission and distribution - T&D), storage, and customers. Modern society enjoys several devices and technologies from fast media communication to work, cooking, health, security, and others; all these intrinsically depend on electrical energy. Nowadays, the scarcity of fossil fuels and the environmental hazards related to their use pave the way for the search for renewable energies. The eolic or photonic sources stand out as exciting alternatives in this context. Another critical issue lies in increasing the efficiency of electrical transport and distribution between power plants and consumers. The metallic wires commonly applied in the T&D show an electrical loss during electronic transport due to the thermal energy dissipation or heating, as predicted by the Joule effect. Therefore, a material with a minor loss to transport electrons is essential to optimize the generated energy delivery [1–2].

Nowadays, the research on superconductor materials is a great promise to contribute to T&D because of a perfect transmission without the energy dissipation during the electrical current being able to revolutionize electrical efficiency for T&D. Quantum effects rising inside of these materials make the thermal energy dissipation disappear (null Joule effect). In particular, the electrons runway freely in the superconductor because the vibrational modes are deeply reduced from the shallow temperature causing a decoupling between electronic and vibrational modes. The reduced vibrational degrees of freedom of the crystalline structure allows the superconductors superior conductance. Recently, the charge density wave (CDW) phase and topological phenomena discuss the intriguing electronic properties connected to electrical conductivity in the superconductor state [3] of the Transition metal dichalcogenide (TMDs) materials. CDW, initially proposed in the 1930 s by Rudolf Peierls, shows that the electronic state of unidimensional (1D) or quasi-bidimensional (quasi-2D) materials forms an unstable band gap at Fermi energy (E_F) below a particular temperature denominated as Peierls temperature (T_P). The propagation of the CDW is a flux of electrons propagated as a wave in the quantum level inside the crystalline lattice; the spin moment creates different CDW causing waves modulation in 180° out-of-phase between the two phases.

* Corresponding author.
E-mail address: srlazaro@uepg.br (S.R. de Lazaro).

https://doi.org/10.1016/j.commatsci.2022.111672
Received 7 February 2022; Received in revised form 27 June 2022; Accepted 15 July 2022
Available online 4 August 2022

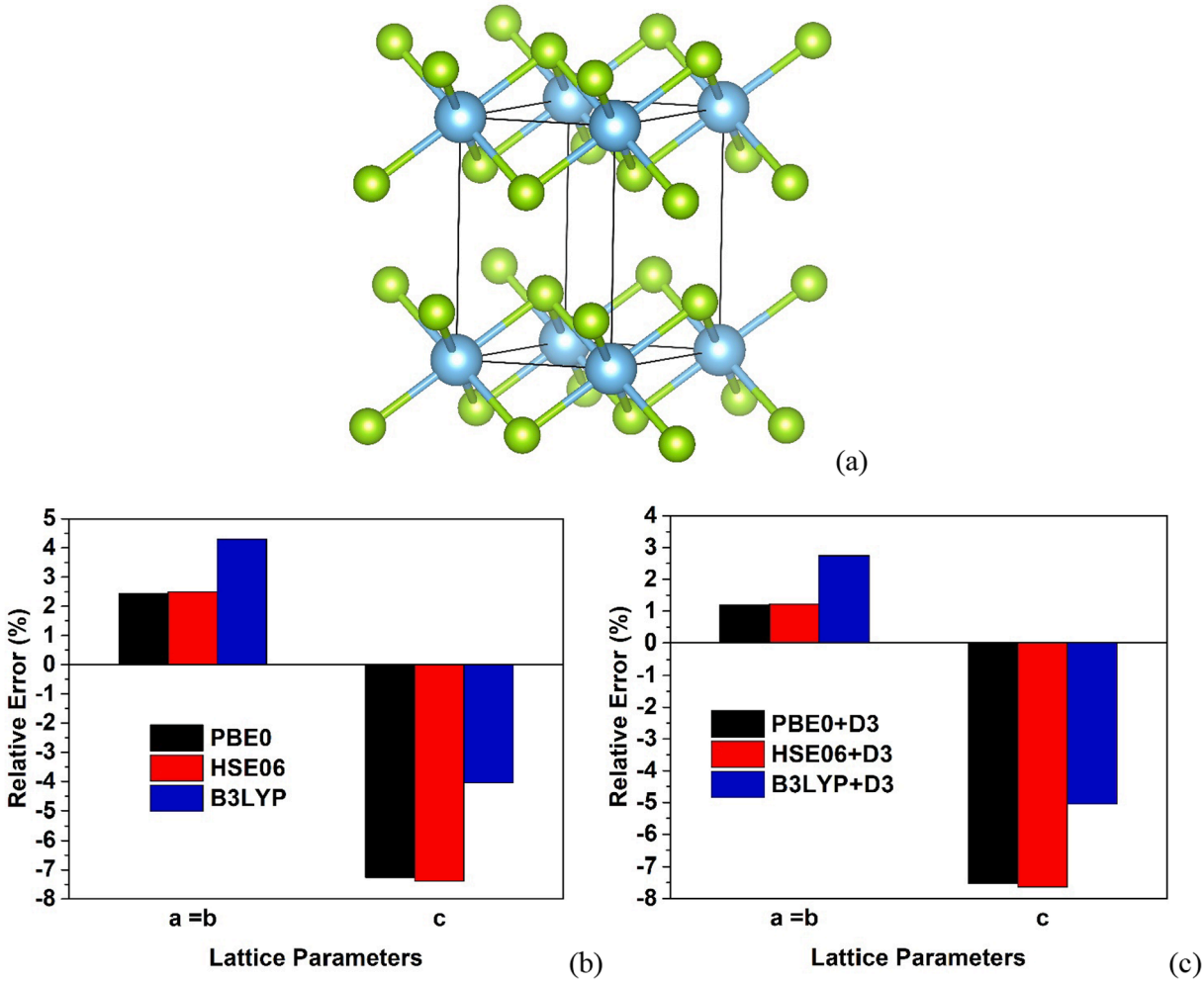

Fig. 1. (a) Lamellar structure by the pristine spatial arrangement characteristic of the space group *P*-3*m1* presents in the $TiSe_2$ material. Relative errors in % calculated for the lattice parameters of the *P*-3*m1* pristine $TiSe_2$ material from PBE0, HSE06, and B3LYP functionals (b) and Grimme's dispersion (D3) (c). Positive and negative values overestimate and underestimate the experimental data, respectively.

Table 1
Lattice parameters in Å calculated for the *P*-3*m1* pristine $TiSe_2$ structure from PBE0, B3LYP, and HSE06 functionals and D3 dispersion correction. Relative errors are in parenthesis.

Functional	a = b	c
PBE0	3.621 (2.4 %)	5.572 (-7.3 %)
HSE06	3.623 (2.5 %)	5.564 (-7.4 %)
B3LYP	3.687 (4.3 %)	5.765 (-4.0 %)
Exp. *	3.536	6.008
PBE0+D3	3.577 (1.2 %)	5.556 (-7.5 %)
HSE06+D3	3.578 (1.2 %)	5.549 (-7.6 %)
B3LYP+D3	3.632 (2.7 %)	5.705 (-5.0 %)

* Ref. [19].

The high-temperature superconductors such as $YBa_2Cu_3O_{7-\delta}$ (YBCO) have the CDW effect associated with superconductivity property, being the massive electrical conduction near T_P the driven force for an extensive discussion in the literature [4].

TMDs exhibit excellent electronic properties, suitable as semiconductors and superconductors. The chemical composition of the TMDs is MX_2, where M is a transition metal (M = Mo, W, Nb, Ta, Ti) and X a chalcogenide atom (X = S, Se, Te), composing a lamellar arrangement or quasi-2D materials [3–4]. The lamellar structure has a high van der Waals contribution causing the modulation of the electronic properties, while the M–X bonds possess a strong covalent character [5]. Each bidimensional structure or "sandwich" characterizes a plane of M atoms into two other chalcogenide atoms plans. Six chalcogenide atoms coordinated with one transition metal, $[MX_6]$ clusters, forming an octahedral geometry along with the *P*-3*m1* space group in the 1 T phase and trigonal prismatic clusters in P_{63}/mmc space group for the 2H phase. TMDs superconductors present superconductor type-2 with an anisotropic character in electronic conductivity in Ti–Ti plane [6–8]. The $TiSe_2$ material presents a quasi-2D arrangement, a superconductor state near 4.4K, and a CDW effect. In such CDW model for quasi-2D materials, the Cooper's pair is the wave that creates the high electrical transport without energy dissipation [9].

The computational chemistry applied in theoretical calculations based on quantum mechanics is widely used to elucidate electronic properties in solid-state materials and propose new materials or physical models to describe electronics phenomena [10–11]. To describe TMDs by computational methods in Density Functional Theory (DFT), the exchange–correlation functional must describe the covalent bonds present in the material satisfactorily. Therefore, the study of exchange–correlation functional in TMDs materials is essential because the formalism of each functional changes significantly to represent complex electronic structures in the chemical compounds [12–13]. The exchange–correlation functional of the electronic density (ρ) is the key point in DFT, the analytic global function to satisfy the derivative form is unknowledge until present moment. Moreover, the Generalized Gradient Approximation (GGA) is the successful approach to build

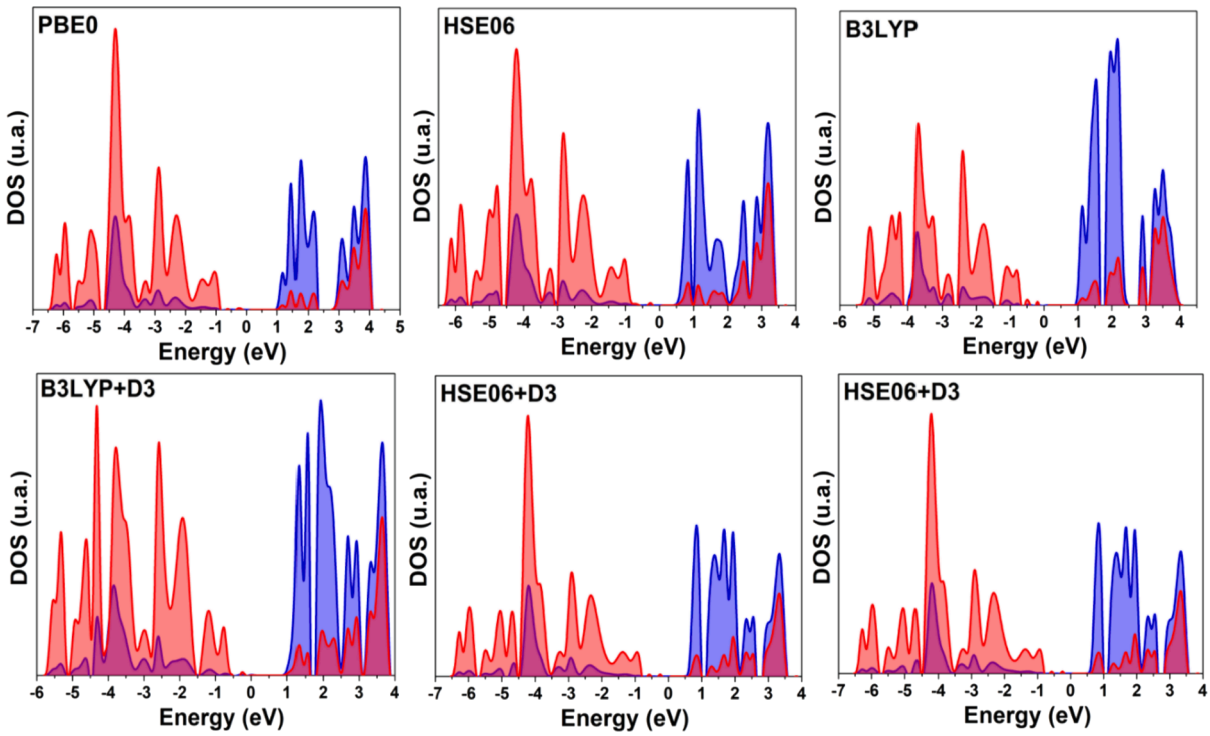

Fig. 2. Density of States (DOS) profiles calculated from PBE0, HSE06, and B3LYP functionals and Grimme's dispersion (D3) on Se (red) and Ti (blue) atoms. The Valence Band (VB) are electronic states below 0eV, and the Conduction Band (CB) electronic states above 0eV. The Fermi energy was fixed in 0 eV. (For interpretation of the references to colour in this figure legend, the reader is referred to the web version of this article.)

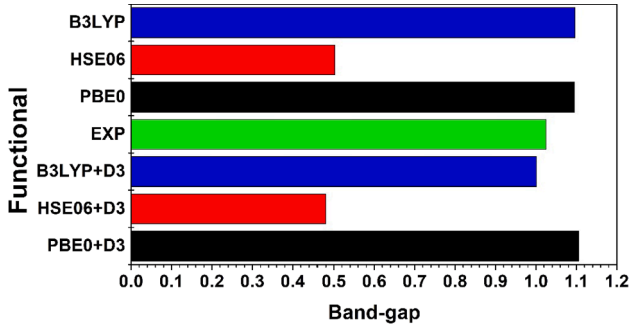

Fig. 3. Relative errors in % calculated for the lattice parameters of the $TiSe_2$ pristine material from PBE0, HSE06, and B3LYP functionals and Grimme's dispersion (D3). Positive and negative values overestimate and underestimate the experimental data, respectively.

mathematic functions for the functionals used in DFT. Hybrid functionals are a big functional family, which inserted part of Hartree-Fock exchange (HF_x) term from a linear combination into functional formalism in the DFT. Then, the Perdew-Burke-Ernzerhof (PBE0) [14], Becke functional three-parametrized by Lee-Yang-Parr (B3LYP) [15–16], and Krukau-Vydrov-Izmaylov-Scuseria (HSE06) [17] belong hybrid functionals family with own features. PBE0 has incorporated a pure HF_x term as an independent term at 3:1 ratio classified as hybrid functional, while the B3LYP developed thermodynamic coefficients and local spin density approximation called as parametrized hybrid functional, and the HSE06 is a hybrid functional because it applies an error-function-screened Coulomb potential on exchange term.

In this work, DFT simulations using the PBE0, B3LYP, and HSE06 hybrid functionals simulate the $TiSe_2$ material aiming to investigate the influence of the D3 dispersion correction on the structural and electronic properties.

Table 2
Vibrational modes calculated from PBE0, HSE06, and B3LYP functionals and Grimme's dispersion (D3) in cm^{-1} for the Ti–Ti, Se–Se, and Ti–Se chemical bonds.

Functionals	Ti – Ti	Se – Se	Se – Se	Ti – Se
PBE0	97.78 (25.0 %)	168.78 (22.0 %)	227.14 (10.0 %)	346.12 (0.3 %)
HSE06	84.74 (9.0 %)	167.71 (22.0 %)	225.99 (10.0 %)	342.16 (-0.8 %)
B3LYP	34.44 (-55.0 %)	160.07 (16.0 %)	216.84 (5.0 %)	321.74 (-7.0 %)
Exp.*	78 (E_g)	138 (E_g)	206 (A_{1g})	345 (A_u)
PBE0+D3	67.50 (-14.0 %)	174.20 (26.0 %)	245.59 (19.0 %)	353.89 (3.0 %)
HSE06+D3	37.01 (-53.0 %)	173.08 (25.0 %)	244.18 (19.0 %)	394.76 (14.0 %)
B3LYP+D3	0.0 (-100.0 %)	168.11 (22.0 %)	241.48 (17.0 %)	331.94 (-4.0 %)
Activity / Symmetry	IR / E_u	Raman / E_g	Raman / A_{1g}	IR / A_{2u}

* Ref. [32].

2. Computational methods

The experimental results [19] for the *P-3m1* unit cell indicates a = b = 3.536Å, c = 6.008Å, α = β = 90°, and γ = 120° with internal positions of Ti (0.0; 0.0; 0.0), Se (0.333; 0.667; 0.231), and Se (0.667; 0.333; 0.769). In the 1T pristine structure (Fig. 1), Ti atoms are surrounded by six Se atoms in octahedral geometry with a 1T phase. The van der Waals separation between two Se–Ti–Se adjacent layers is closer to 3.5Å. The Ti and Se atoms were described by 8–6411(d311f) [20] and m-pVDZ-PP [21] Gaussian basis sets, respectively. Computational simulations for the 1T $TiSe_2$ material were carried out from DFT to evaluate the performance of the PBE0 (hybrid) [14], B3LYP (parameterized hybrid) [15–16], and HSE06 (hybrid) [17] exchange–correlation functionals.

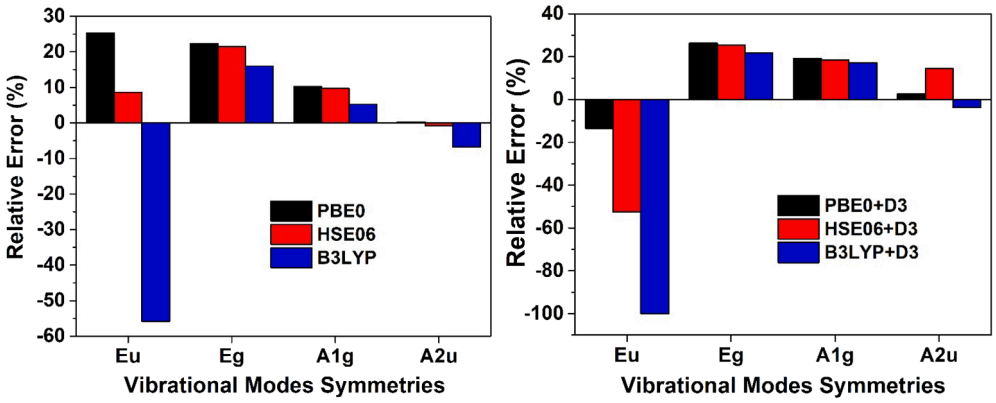

Fig. 4. Relative errors in % calculated for the lattice parameters of the $TiSe_2$ pristine material from PBE0, HSE06, and B3LYP functionals and Grimme's dispersion (D3). Positive and negative values overestimate and underestimate the experimental data, respectively.

The CRYSTAL17 code was used for periodic quantum simulations performed in this work. A posteriori dispersion energy correction was considered based on the model developed by Grimme *et al* [18] denominated as D3. The bulk dimension was the choice to represent the periodic expansion of the crystalline lamellar structure. The convergence criteria for mono- and bielectronic integrals were both set to 10^{-8} Hartree, while the convergence method was the root-mean-square (RMS), the maximum gradient and maximum displacement were set to 3×10^{-4}, 1.2×10^{-4}, 4.5×10^{-5}, and 1.8×10^{-4} a.u., respectively. The convergence criterium between optimization steps was the default in 10^{-7} a.u. Regarding the density matrix diagonalization, the reciprocal space net was described by a shrinking factor set to $4 \times 4 \times 4$, corresponding to 27 k-points following the Monkhorst-Pack method. The computational time measure for computational costs from output of the electronic calculations were 3700.59 s for PBE0, 15310.45s for HSE06, 2452.70s B3LYP, 2623.19s for PBE0+D3, 11638.94s for HSE06+D3, and 2208.47s B3LYP+D3. While, for vibrational modes calculations were 2915.47s for PBE0, 15153.78s for HSE06, 2502.72s B3LYP, 2738.15s for PBE0+D3, 13888.93s for HSE06+D3, and 2488.71s B3LYP+D3. Quadricore processors ran all quantum DFT simulations above.

3. Results and discussion

3.1. Structural parameters

Computational simulations on solid-state reached a high level from the DFT approach in the last years [22–24], corroborating with experimental results to predict structural and electronic properties. The calculated structural parameters strongly agree with X-ray Diffraction data [19]. Table 1 shows the lattice parameters and the relative error (Eq. (1)) associated with experimental data. The PBE0 and HSE06 functionals presented more accuracy on a and b lattice parameters or plane dimensions and less precision in the c lattice parameter. In other words, these functionals describe more precisely the exchange–correlation effect on electronic interactions in a short distance (into the identical lamella or sandwich); whereas for long-distance (weak interactions as van der Waals forces) between Se–Se atoms, the description is a poor. The relative error (Eq. (1)) was applied to evaluate the theoretical results (R_{DFT}) deviation from the experimental data (R_{exp}). Positive relative errors are overestimated deviations from experimental data, while negative relative errors are underestimated deviations from experimental data.

$$error(\%) = \frac{R_{DFT} - R_{exp}}{R_{exp}} x100 \quad (1)$$

Including thermochemistry data in the B3LYP formalism is responsible for correcting the exchange–correlation energy, better describing the attractive effect at long distance or Se–Se interlayer distance, 3.363Å. D3 dispersion increased the accuracy substantially in-plane dimension; however, the correction was negligible in the c lattice parameter. For the B3LYP+D3, the relative errors were similar for the B3LYP. The c lattice parameter was calculated more accurately than other functionals, indicating an influence of the thermochemical parametrization included inside B3LYP formalism. Furthermore, the Grimme's dispersion reduces the calculated values for a and b lattice parameters.

In the previous theoretical report [25], the TiO_2 material in anatase and rutile phases and graphite were evaluated on the PBE0 and B3LYP functionals with Grimme's dispersion. The results of the functionals for these materials showed the increase of the covalent part on the chemical bond, i.e., Ti–O and C═C bonds, enhanced the relative error along z-direction for PBE0, and the D3 dispersion correction effects majorly affect the planar(x,y) interactions. Then, for TiO_2 and graphite, the anisotropic effect localized on the z-direction is poorly modified by Grimme's dispersion. Here, a similar behavior was denoted for the $TiSe_2$ lamellar material. Since the O and Se atoms have the same chemical group (chalcogenide), the high difference in electronegativity indicates structural modifications regarding the TiO_2 (non-lamellar). In this fact, the introduction of the dispersion contributed in a low scale to represent the anisotropic effect under the c lattice parameter confirming the tendency noted on the TiO_2. The high distance between the $TiSe_2$ "sandwiches" is the reason behind the low description.

Fig. 1 shows the relative error modulation of the lattice parameters for the $TiSe_2$ pristine structure from PBE0, HSE06, and B3LYP functionals and Grimme's dispersion. The B3LYP has more relative error than PBE0 and HSE06 (Fig. 1b) for the a and b lattice parameters; while, for c lattice parameter is opposite, the B3LYP functional was the more accurate. The D3 Grimme dispersion corrected the a and b lattice parameters satisfactorily (Fig. 1c); however, the c lattice parameter was poorly affected. Then, Grimme dispersion influenced more the Se–Ti Se sandwich because the atomic interactions are in the range of the dispersion. The c lattice is predominantly dominated by interlayer distance Se–Se at van der Waals range; such distance was low corrected, keeping similar relative error.

3.2. Electronic profiles

Diffuse functions in Gaussian base sets aim to describe electrons in diffuse behavior as isolated pair or anion states from low linear coefficients allowing mathematical functions for a diffuse electronic density. Such a tool is essential for chemical reactions or molecular interactions very nearby. The long-range interactions, such as van der Waals and London-London effects [26–28], are much more diffused with large distances above 3.0Å. The introduction of the D3 Grimme

dispersion makes it possible to determine the influence of the long-distance interactions on DOS profiles of the $TiSe_2$ material. Then, the long-range description from Grimme's dispersion corrects the electronic descriptions in a space on applied Gaussian basis sets that do not describe the electronic density.

Atomic DOS profiles (Fig. 2) show a similar distribution for all functional states on the Valence Band (VB). The Se 4p atomic states are predominant on 3d Ti atomic states because of electronegativity, causing a spontaneous charge separation. The VB states are essential to indicate electronic excitation processes associated with optical or conductive properties. All DOS projections showed a similar excitation process; the electrons localized on Se atoms can excite Ti atoms, proposing a solid charge transfer as an electronic mechanism. For other materials, this kind of behavior was reported [29–30]. The modulation of the bandgap is an indirect result of the challenge of understanding a phenomenon as complex as the exchange–correlation, which is an acceptable interaction among electrons. For other materials, this kind of behavior was reported [29–30]. Therefore, all calculations successfully described the electronic process, but the quantitative approach is variable because of the exchange–correlation description. The Conduction Band Minimum (CBM) energies were calculated as 1.103eV (PBE0), 0.513eV (HSE06), and 1.109eV (B3LYP). Then, the CBM energies were predicted similarly for PBE0 and B3LYP, and the HSE06 drastically reduced the energy levels connected to virtual states. For the Valence Band Maximum (VBM), the energies are 0.007eV (PBE0), 0.011eV (HSE06), and 0.014eV (B3LYP). Moreover, the high modulation on the CBM for the HSE06 functional caused a high decrease on the bandgap, demonstrating a strong influence in the projection on anti-bonding levels of the $TiSe_2$ material connected on z-direction. The bandgap calculation indicated that the PBE0 and B3LYP functionals predicted in more agreement the experimental result of 1.025eV [31] with an overestimation of 9.95% and 7.02%, respectively, while the HSE06 functional calculated a high underestimation with a relative error of −46.5% (Fig. 3).

The description of the exchange–correlation energies in functionals is essential to the electronic properties. The PBE0 and B3LYP describe the exchange–correlation energy with similar qualitative and quantitative errors and HSE06 functional in the opposite. In both B3LYP and PBE0, the exchange–correlation term is composed of mixing between exact Hartree-Fock (HF_x) and DFT parts, of which the HF_x is 20 and 25%, respectively. From a direct inspection of B3LYP, the thermochemistry parametrization influences the energy levels in Valence Band Maximum (VBM) and the bandgap reduction. Another point is the increase of the HF_x in B3LYP, representing in a more precise way the high HF_x of PBE0. On the other hand, for the HSE06 functional, the amount of HF_x depends on the distance between electrons; the applied HF_x is 25% to short-range interactions, contributing to a higher underestimated bandgap mainly because of the exchange effect in-plane Ti-Se interactions. The introduction of the D3 dispersion modifies the CBM energy levels for 1.097eV (PBE0), 0.518eV (HSE06), and 1.014eV (B3LYP); the B3LYP was more modulated. The values of −0.009eV (PBE0), 0.038eV, and 0.013eV (B3LYP) are the new VBM energy levels, indicating strong modulations for PBE0 and HSE06. Thus, the D3 dispersion changed the VBM energy level of the B3LYP to low, showing that the Grimme's dispersion weakly influences thermochemistry parametrization for $TiSe_2$. The inclusion of a posteriori correction is more pronounced for hybrid functionals with higher HF_x amounts because of the description of the short-range interactions, resulting in essential contributions to such kinds of exchange–correlation treatments.

3.3. Harmonic vibrational modes analysis

Vibrational modes were calculated at 0K and vacuum using the quantum harmonic model. The nuclear stretching modeling occurs close to the minimum of the chemical bond, and high stretching is despised. A pair-to-pair nuclear analysis in stationary points is the general approach to calculating harmonic vibrational modes. Posteriorly, symmetry groups and infrared rules classify the calculated vibrational modes as active or inactive, estimating the intensities. PBE0, HSE06, and B3LYP simulations provide only positive frequencies calculated for harmonic vibrational modes.

The experimental vibrational modes symmetries [32–36] found for the infrared (IR) active modes were E_u ($78cm^{-1}$) + A_{2u} ($345cm^{-1}$); while the Raman modes have E_g ($138cm^{-1}$) + A_{1g} ($206cm^{-1}$) symmetries. The low frequencies (Table 2) in the E_u symmetry were calculated for Ti–Ti stretching with $97.78cm^{-1}$ (PBE0), $84.74cm^{-1}$ (HSE06), and $34.44cm^{-1}$ (B3LYP). The Se–Se equatorial stretching in E_g symmetry are Raman mode calculated as $168.78cm^{-1}$ (PBE0), $167.71cm^{-1}$ (HSE06), and $160.07cm^{-1}$. Another vibrational mode associated with Se–Se stretching carries out equatorial movement with $227.14cm^{-1}$ (PBE0), $225.99cm^{-1}$ (HSE06), and $216.84cm^{-1}$ (B3LYP) frequencies and A_{1g} symmetry. The vibrational modes for the A_{2u} symmetry were $346.12cm^{-1}$ (PBE0), $342.16cm^{-1}$ (HSE06), and $321.74cm^{-1}$ (B3LYP) frequencies connected to an axial movement on the Ti–Se stretching.

The most deviation among DFT functionals is on the low frequencies connected to E_u mode or Ti–Ti stretching; the deviation for other frequencies is satisfactory (Fig. 4). The PBE0 and HSE06 functionals have low relative errors, indicating that both exchange–correlation descriptions are near harmonic vibrational simulations. It is interesting because the description of the HSE06 functional for electronic structure is more than PBE0. The similarity between structural parameters and harmonic vibrational modes between PBE0 and HSE06 functionals indicates that the optimized atomic positions did simulate harmonic vibrational modes nearby. The thermochemical parametrization included in the B3LYP functional was the most important factor for calculating the structural parameters and nuclear positions directly influencing different harmonic vibrational modes. All calculated harmonic vibrational modes decreased from PBE0 > HSE06 > B3LYP. The deviation of the B3LYP was more significant regarding PBE0 or HSE06 functionals.

4. Conclusion

Lattice parameters for *P-3m1* lamellar structure in the $TiSe_2$ material indicated that D3 Grimme's dispersion influenced more in a and b lattice parameters than c lattice parameters, an unexpected fact. In band-gap results, the Hartree-Fock mixing in GGA functionals indicated more agreement with experimental results for PBE0 and B3LYP functionals than HSE06 functional. In general, all functionals failed to estimate low vibrational modes. The B3LYP was the most relative deviation; for more energetic vibration modes, the relative error decreased, and D3 dispersion influenced the vibration modes calculations in the low range. The PBE0 functional successful in describing the evaluated properties.

CRediT authorship contribution statement

Sergio Ricardo de Lazaro: Conceptualization, Methodology, Writing – original draft, Writing – review & editing, Supervision, Project administration, Resources. **Guilherme Bonifácio Rosa:** Visualization. **Renan Augusto Pontes Ribeiro:** Formal analysis, Investigation. **Luis Henrique da Silveira Lacerda:** Formal analysis, Investigation. **Marisa Carvalho de Oliveira:** Formal analysis, Investigation. **Elson Longo:** Supervision.

Declaration of Competing Interest

The authors declare that they have no known competing financial interests or personal relationships that could have appeared to influence the work reported in this paper.

Data availability

No data was used for the research described in the article.

Acknowledgements

This work was supported by Coordenação de Aperfeiçoamento de Pessoal de Nível Superior (CAPES), National Council for Scientific and Technological Development (CNPq) for grant 164266/2020-8, and Fundação Araucária. The authors also acknowledge support from São Paulo Research Foundation (FAPESP) for grants 2013/07296-2, 2016/23891-6, 2017/26105-4, 2021/01651-1, and 2020/03780-0.

References

[1] H. Hosono, K. Kuroki, Iron-based superconductors: Current status of materials and pairing mechanism, Phys. C Supercond. 514 (2015) 399–422, https://doi.org/10.1016/j.physc.2015.02.020.
[2] H. Liao, J.V. Milanović, Techno-economic analysis of global power quality mitigation strategy for provision of differentiated quality of supply, Int j. electr. power energy syst. 107 (2019) 159–166, https://doi.org/10.1016/j.ijepes.2018.11.006.
[3] W. Shi, B.J. Wieder, H.L. Meyerheim, Y. Sun, Y. Zhang, Y. Li, L. Shen, Y. Qi, L. Yang, J. Jena, P. Werner, K. Koepernik, S. Parkin, Y. Chen, C. Felser, B. A. Bernevig, Z. Wang, A charge-density-wave topological semimetal, Nat. Phys. 17 (3) (2021) 381–387, https://doi.org/10.1038/s41567-020-01104-z.
[4] X. Zhu, Y. Cao, J. Zhang, E.W. Plummer, J. Guo, Classification of charge density waves based on their nature, PNAS 112 (8) (2015) 2367–2371, https://doi.org/10.1073/pnas.1424791112.
[5] M.K. Hooda, C.S. Yadav, D. Samal, Electronic and topological properties of group-10 transition metal dichalcogenides, J. Phys.: Condens. Matter. 33 (10) (2021) 103001, https://doi.org/10.1088/1361-648X/abd0c2.
[6] S. Manzeli, D. Ovchinnikov, D. Pasqier, O.V. Yazyev, A. Kis, 2D transition metal dichalcogenides, Nat. Rev. Mater. 2 (2017) 17033, https://doi.org/10.1038/natrevmats.2017.33.
[7] A.R. Jurelo, R.A.P. Ribeiro, S.R. de Lazaro, J.F.H.L. Monteiro, Structural, vibrational and electronic properties of the superconductor Cu_xTiSe_2: theoretical and experimental insights, Phys. Chem. Chem. Phys. 20 (42) (2018) 27011–27018.
[8] M. Sasaki, A. Ohnishi, T. Kikuchi, M. Kitaura, Ki-Seok Kim, Heon-Jung Kim, Interplay between the Kondo effect and randomness: Griffiths phase in MxTiSe2 (M=Co, Ni, and Fe) single crystals, Phys. Rev. B 82 (2010), 224416, https://doi.org/10.1103/PhysRevB.82.224416.
[9] A. Chikina, A. Fedorov, D. Bhoi, V. Voroshnin, E. Haubold, Y. Kushnirenko, K. H. Kim, S. Borisenko, Turning charge-density waves into Cooper pairs, npj Quantum Mater. 5 (2020) 22, https://doi.org/10.1038/s41535-020-0225-5.
[10] S. Kezilebieke, M.N. Huda, P. Dreher, I. Manninen, Y. Zhou, J. Sainio, R. Mansell, M.M. Ugeda, S. van Dijken, H. Komsa, P. Liljeroth, Electronic and magnetic characterization of epitaxial VSe_2 monolayers on superconducting $NbSe_2$, Commun. Phys. 3 (2020) 116, https://doi.org/10.1038/s42005-020-0377-4.
[11] A. Du, Z. Pendergrast, S. Barraza-Lopez, Tuning energy barriers by doping 2D group IV monochalcogenides, J. Appl. Phys. 127 (23) (2020) 234103, https://doi.org/10.1063/5.0008502.
[12] R.A.P. Ribeiro, S.R. de Lazaro, C. Gatti, The role of exchange–correlation functional on the description of multiferroic properties using density functional theory: the $ATiO_3$ (A = Mn, Fe, Ni) case study, RSC Adv. 6 (103) (2016) 101216–101225.
[13] C. Zhao, D. Wang, R. Lian, D. Kan, Y. Dou, C. Wang, G. Chen, Y. Wei, Revealing the distinct electrochemical properties of $TiSe_2$ monolayer and bulk counterpart in Li-ion batteries by first-principles calculations, Appl. Surf. Sci. 540 (2021) 148314, https://doi.org/10.1016/j.apsusc.2020.148314.
[14] J.P. Perdew, K. Burke, M. Ernzerhof, Generalized gradient approximation made simple, Phys. Rev. Lett. 77 (18) (1996) 3865–3868, https://doi.org/10.1103/PhysRevLett.77.3865.
[15] A.D. Becke, Density-functional thermochemistry. III. The role of exact exchange, J. Chem. Phys. 98 (7) (1993) 5648–5652, https://doi.org/10.1063/1.464913.
[16] C. Lee, W. Yang, R.G. Parr, Development of the Colle-Salvetti correlation-energy formula into a functional of the electron density, Phys. Rev. B. 37 (2) (1988) 785–789.
[17] A.V. Krukau, O.A. Vydrov, A.F. Izmaylov, G.E. Scuseria, Influence of the exchange screening parameter on the performance of screened hybrid functionals, J. Chem. Phys. 125 (22) (2006) 224106, https://doi.org/10.1063/1.2404663.
[18] S. Grimme, J. Antony, S. Ehrlich, H. Krieg, A Consistent and Accurate ab Initio Parametrization of Density Functional Dispersion Correction (DFT-D) for the 94 Elements H-Pu, J. Chem. Phys. 132 (15) (2010) 154104, https://doi.org/10.1063/1.3382344.
[19] W.G. Stirling, B. Dorner, J.D.N. Cheeke, J. Revelli, Acoustic phonons in the transition-metal dichalcogenide layer compound, $TiSe_2$, Solid State Commun. 18 (7) (1976) 931–933, https://doi.org/10.1016/0038-1098(76)90240-4.
[20] A. Erba, K.E. El-Kelany, M. Ferrero, I. Baraille, M. Rérat, Piezoelectricity of $SrTiO_3$: An ab initio description, Phys. Rev. B. 88 (2013), 035102, https://doi.org/10.1103/PhysRevB.88.035102.
[21] P. Pernot, B. Civalleri, D. Presti, A. Savin, Prediction Uncertainty of Density Functional Approximations for Properties of Crystals with Cubic Symmetry, J. Phys. Chem. A. 119 (21) (2015) 5288–5304, https://doi.org/10.1021/jp509980w.
[22] M. Ricci, A. Ambrosetti, P.L. Silvestrelli, Improving the Description of Interlayer Bonding in TiS_2 by Density Functional Theory, J. Phys. Chem. C. 124 (50) (2020) 27592–27603, https://doi.org/10.1021/acs.jpcc.0c09460.
[23] M.C. Oliveira, J. Andrés, L. Gracia, M.S.M.P. de Oliveira, J.M.R. Mercury, E. Longo, I.C. Nogueira, Geometry, electronic structure, morphology, and photoluminescence emissions of $BaW_{1-x}Mo_xO_4$ (x = 0, 0.25, 0.50, 0.75, and 1) solid solutions: Theory and experiment in concert, Appl. Surf. Sci. 463 (2019) 907–917.
[24] L.H.d.S. Lacerda, E. Longo, J. Andrés, M.A. San-Miguel, A diagnosis approach for semiconductor properties evaluation from ab initio calculations: Ag-based materials investigation, J. Solid State Chem. 305 (2022) 122670, https://doi.org/10.1016/j.jssc.2021.122670.
[25] L. K. Andreani, *et al*; Engineering Materials. Springer, Cham.; Emerging Research in Science and Engineering Based on Advanced Experimental and Computational Strategies, 341–357 (2020). https://doi.org/10.1007/978-3-030-31403-3_1.
[26] J. Clerk-maxwell, O ver de continuiteit van den gas- en vloeistofiocstand Academisch proefschrift, Nature. 10 (259) (1874) 477–480, https://doi.org/10.1038/010477a0.
[27] H. Margenau, Van der Waals forces, Rev. Mod. Phys. 11 (1) (1939) 1–35, https://doi.org/10.1103/RevModPhys.11.1.
[28] S. Kawai, A. Foster, T. Björkman, S. Nowakowska, J. Björk, F.F. Canova, L.H. Gade, R.A. Jung, E. Meyer, Van der Waals interactions and the limits of isolated atom models at interfaces, Nat. Commun. 7 (2016) 11559, https://doi.org/10.1038/ncomms11559.
[29] R.L. Tranquilin, M.C. Oliveira, A.A.G. Santiago, L.X. Lovisa, R.A.P. Ribeiro, E. Longo, S.R. de Lazaro, C.R.R. Almeida, C.A. Paskocimas, F.V. Motta, M.R. D. Bomio, Presence of excited electronic states on terbium incorporation in $CaMoO_4$: Insights from experimental synthesis and first-principles calculations, J. Phys. Chem. Solids 149 (2021) 109790, https://doi.org/10.1016/j.jpcs.2020.109790.
[30] A.A.G. Santiago, M.C. Oliveira, R.A.P. Ribeiro, R.L. Tranquilin, E. Longo, S.R. de Lázaro, F.V. Motta, M.R.D. Bomio, Atomistic Perspective on the Intrinsic White-Light Photoluminescence of Rare-Earth Free $MgMoO_4$ Nanoparticles, Cryst. Growth Des. 20 (10) (2020) 6592–6603, https://doi.org/10.1021/acs.cgd.0c00757.
[31] H. Saqib, S. Rahman, Y. Zhao, C. Cazorla, D. Errandonea, R. Susilo, Y. Zhuang, Y. Huang, B. Chen, N. Dai, Evolution of Structural and Electronic Properties of $TiSe_2$ under High Pressure, J. Phys. Chem. Lett. 12 (40) (2021) 9859–9867, https://doi.org/10.1021/acs.jpclett.1c02492.
[32] J.A. Holy, K.C. Woo, M.V. Klein, F.C. Brown, Raman and infrared studies of superlattice formation in $TiSe_2$, Phys. Rev. B 16 (8) (1977) 3628–3637, https://doi.org/10.1103/PhysRevB.16.3628.
[33] J.A. Wilson, A.S. Barker, F.J. Di Salvo Jr, J.A. Ditzenberger, Infrared properties of the semimetal $TiSe_2$, Phys. Rev. B. 18 (6) (1978) 2866, https://doi.org/10.1103/PhysRevB.18.2866.
[34] S. Sugai, K. Murase, S. Uchida, S. Tanaka, Raman studies of lattice dynamics in 1T-$TiSe_2$, Solid State Commun. 35 (5) (1980) 433–436, https://doi.org/10.1016/0038-1098(80)90175-1.
[35] H. Cercellier, C. Monney, F. Clerc, C. Battaglia, L. Despont, M.G. Garnier, H. Beck, P. Aebi, L. Patthey, H. Berger, L. Forró, Evidence for an Excitonic Insulator Phase in 1T−$TiSe_2$, Phys. Rev. Lett. 99 (2007), 146403, https://doi.org/10.1103/PhysRevLett.99.146403.
[36] M. Hellgren, J. Baima, R. Bianco, M. Calandra, F. Mauri, L. Wirtz, Critical Role of the Exchange Interaction for the Electronic Structure and Charge-Density-Wave Formation in $TiSe_2$, Phys. Rev. Lett. 119 (2017), 176401, https://doi.org/10.1103/PhysRevLett.119.176401.